IEEE Access
Multidisciplinary | Rapid Review | Open Access Journal

Received November 12, 2020, accepted November 21, 2020, date of publication December 1, 2020,
date of current version December 11, 2020.

Digital Object Identifier 10.1109/ACCESS.2020.3041794

Bifurcation Control in an Optimal Velocity Model via Double Time-Delay Feedback Method

WEILIN REN[1,2,3], RONGJUN CHENG[1,2,3], HONGXIA GE[1,2,3], AND QI WEI[4]
[1]Faculty of Maritime and Transportation, Ningbo University, Ningbo 315211, China
[2]Jiangsu Province Collaborative Innovation Center of Modern Urban Traffic Technologies, Nanjing 210096, China
[3]National Traffic Management Engineering and Technology Research Centre Ningbo University Sub-Center, Ningbo 315211, China
[4]Department of Logistics Management, Ningbo University of Finance and Economics, Ningbo 315175, China

Corresponding author: Rongjun Cheng (chengrongjun@nbu.edu.cn)

This work was supported in part by the Ningbo Natural Science Foundation of China under Grant 202003N4142 and Grant 2019A610048, and in part by the K. C. Wong Magna Fund in Ningbo University, China.

ABSTRACT In this paper, a double time-delay feedback control of an optimal velocity model (OVM) is investigated. Double time-delay means that there exist two different state feedback control signals in the controlled OVM system, which are related to the velocity difference and the optimal velocity difference, respectively. Through linear stability analysis, the critical condition of Hopf bifurcation for the controlled OVM is derived. Utilizing the characteristics of Hopf bifurcation and the improved definite integral method, appropriate double time-delay feedback control strategy is designed in term of the number of unstable eigenvalues of the characteristic equation to suppress the stop-and-go waves generated by the uncontrolled OVM. Note that when the number of unstable eigenvalues is equal to zero, the controlled OVM is stable, otherwise, it is unstable. Numerical simulations are executed to validate the accuracy and feasibility of the design of double time-delay control strategy. Finally, case studies approximating the actual traffic situation are given, and the appropriate combination of control parameters is selected through the verified design steps. In addition, the measured data from NGSIM are also considered.

INDEX TERMS Optimal velocity model, double time-delay control, definite integral method, stability analysis, Hopf bifurcation.

I. INTRODUCTION

Time delays have a non-negligible impact on the evolution of traffic flow and driving performance whether human-driven vehicles or self-driven vehicles, which is still a worthy issue for discussion. In recent years, in order to further explore and interpret the sophisticated traffic flow phenomenon caused by time delays, many related traffic flow models have been proposed, including car-following models [1]–[3], continuum models [4]–[6], lattice hydrodynamic models [7], [8].

In 1958, car following model with time delay was presented for the first time by Chandler *et al.* [9] based on classical car following model [10]:

$$\ddot{x}_n(t) = \lambda\left[\dot{x}_{n+1}(t-\tau) - \dot{x}_n(t-\tau)\right] \tag{1}$$

where $\dot{x}_n(t)$ and $\ddot{x}_n(t)$ stand for the speed and acceleration of the nth vehicle, respectively; λ is the driver's sensitivity coefficient; τ is time delay regarding the driver's response to the stimulus. It was found that when $\tau\lambda > 0.5$ (where the unit of τ is seconds and the unit of λ is the reciprocal of seconds), the model would be deprived of stability, which further illustrated that time delay can exert a significant influence on the asymptotic stability of traffic flow. However, the classic car-following model with time delays disregarded the dynamic relationship between traffic flow variables, the sophisticated dynamic evolution of traffic flow cannot be well interpreted. In addition, the classic car-following model only contains velocity terms, without considering the safety distance, so it is easy to cause collision. In order to eliminate this defect, Bando *et al.* [11] proposed an optimal velocity model (OVM) integrating response time delay based on the assumptions that the driver can adjust the speed to the corresponding optimal speed:

$$\ddot{x}_n(t) = a\left[V\left(\Delta x_n(t-\tau)\right) - \dot{x}_n(t-\tau)\right] \tag{2}$$

$$V\left(\Delta x_n\right) = 16.8\left[\tanh\left(0.086\left(\Delta x_n - 25\right)\right) + 0.913\right] \tag{3}$$

The associate editor coordinating the review of this manuscript and approving it for publication was Keli Xiao.

where $\Delta x_n(t) = x_{n+1}(t) - x_n(t)$ represents the headway of the nth vehicle; a is the driver's sensitivity coefficient; $V(\cdot)$ denotes optimal velocity function, which is fitted by the measured data; τ is time lag, containing driver response and mechanical time lag. Through theoretical analysis and numerical simulation, a value representing critical time delay for inducing traffic congestion is obtained, and traffic congestion occurs when the time delay is greater than the critical value. Compared with the classical car following model, OVM can more accurately describe the formation of traffic congestion, stop-and-go waves and other dynamic characteristics. Thereby various improvements to OVM are made to discuss more sophisticated traffic phenomena induced by time delays. Especially, for example, Hopf bifurcation, when a certain parameter in the traffic system exceeds the critical value, the system stability changes suddenly, which has aroused the interest of some traffic scholars [12]–[16]. For example, by considering an OVM with time delay, Igarashi [12] found that there coexist three exact solutions in a certain density range, representing a metastable uniform flow, a metastable congested flow and an unstable congested flow, respectively, which further verified the existence of subcritical bifurcation through numerical tests. Orosz *et al.* [13] implemented bifurcation analysis on a nonlinear car-following model with peculiar attention to driver's reaction-time delay. Their results demonstrated that Hopf bifurcation can give rise to a transformation in stability where oscillations suddenly occur. Moreover, the existence of subcritical bifurcation may bring about bistability between traffic jam and uniformly flowing. Considering that the smaller the distance between adjacent cars in actual traffic, the smaller the driver's reaction-time delay, that is, the driver's reaction time delay is related to the distance between adjacent vehicles Gasser *et al.* [14] introduced variable reaction time delay into the OVM model, and then the bifurcation behavior in the case of variable reaction time delay was shown. In the process of investigating the bifurcation characteristics of a platoon of vehicles, Kamath *et al.* [15] proposed an improved OVM model with attention to delayed feedback. Specially, they proved that the stability analysis results agreed well with the Hopf bifurcation boundary. Moreover, the existence of limit cycles was also proved from a theoretical perspective. Zhang *et al.* [16] presented an extended OVM accounting for time-delayed velocity difference. Similarly, their experimental results also showed that the occurrence of Hopf bifurcation will destroy the stability of traffic flow. However, it is worth mentioning that the delay can also significantly defer the emergence of Hopf bifurcation, as shown in numerical simulation.

From the abovementioned literatures on time delays, it is obvious that time delays can induce the occurrence of bifurcation, while we also find that time delay can also defer the generation of bifurcation, as reflected in Ref. [16]. Hence, how to design an appropriate time delay is an issue worthy of study. At present, most of designs of time delay mainly focus on the design of delay feedback terms [17], [18]. For example, Jin and Hu [17] added new control terms consisting of time-delayed distance and velocity difference into the OVM to alleviate abnormal traffic fluctuations caused by OVM. Considering the popularity of V2V communication, Peng *et al.* [18] constructed a new delay control term based on OVM, involving the two vehicles ahead. Most of the existing researches pay more attention to the overall design of the delay control term while ignoring the delay itself. Moreover, previous time-delay control methods lack flexibility, which can be well applied to the design of a single delay, while for multiple time delays, the stability analysis with respect to delays is limited by the infinite phase space. Combining the characteristics of Hopf bifurcation, Jin *et al.* [19] gave a novel algorithm to accurately calculate the stable delay interval, which gives us an inspiration for the design of delay feedback control.

The subject of this paper is to determine the appropriate combination of parameters for double time-delay feedback control to stabilize traffic flow by utilizing the properties of bifurcation. The remainder of this paper is structured as follows. The OVM with double time-delay control is introduced in Section II. In Section III, the stability analysis on the controlled OVM is conducted to derive the stability criteria. In Section IV, the detailed design steps of double time-delay control are given and the effect of multiple control combinations is tested. In Section V, the design of double time-delay control strategy involving more vehicles is considered as case studies, in which the measured data are also included. Finally, in Section VI, some conclusions are drawn. The research process is represented by the main flowchart shown in Fig.1.

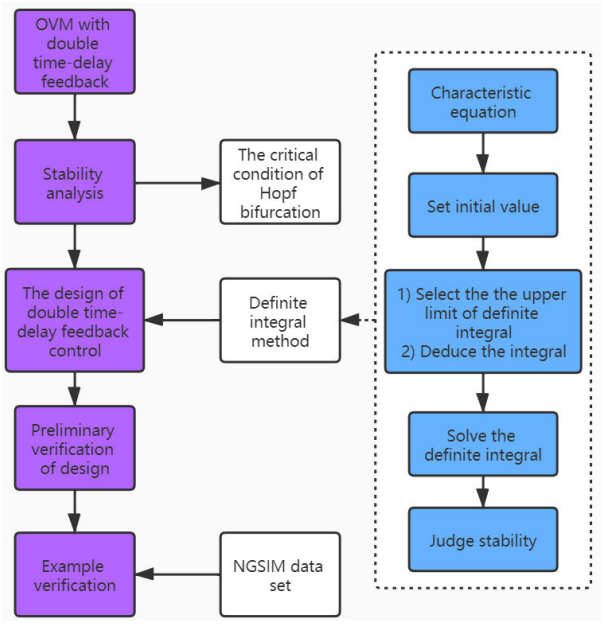

FIGURE 1. Flowchart of research process.

II. THE CONTROLLED OVM

As one of the most widely applied car-following models, OVM [11] can be calculated analytically with the existing

mature differential equation theory, whose stability conditions can be easily obtained. Moreover, some real traffic phenomena and nonlinear characteristics are simulated, such as traffic instability, stagnant traffic, stop-and-go waves. In this paper, a double time-delayed feedback control is proposed to alleviate the traffic congestion produced by the uncontrolled OVM:

$$\frac{dv_n(t)}{dt} = \alpha\left[V\left(\Delta x_n(t)\right) - v_n(t)\right] + \tilde{u}_n(t-\tau_1) + \tilde{e}_n(t-\tau_2) \tag{4}$$

where $\tilde{u}_n(t-\tau_1)$ and $\tilde{e}_n(t-\tau_2)$ denote two different control signals related to time delay which are expressed as follows:

$$\tilde{u}_n(t-\tau_1) = \gamma_1\left[v_n(t) - v_n(t-\tau_1)\right] \tag{5}$$

$$\tilde{e}_n(t-\tau_2) = \gamma_2\left[V\left(\Delta x_n(t)\right) - V\left(\Delta x_n(t-\tau_2)\right)\right] \tag{6}$$

where γ_1 and γ_2 represent the feedback gains of velocity and optimal velocity difference, respectively; τ_1 and τ_2 denote time delays corresponding to delayed-feedback control signal of velocity and optimal velocity difference, respectively. $V\left(\Delta x_n(t)\right)$ is the optimal velocity function which is expressed as follows [20]:

$$V\left(\Delta x_n(t)\right) = 16.8\left[\tanh\left(0.086\left(\Delta x_n(t) - 25\right)\right) + 0.913\right] \tag{7}$$

When $\gamma_2 = 0$, (4) is reduced to the model in Ref. [19]. When $\gamma_1 = \gamma_2 = 0$, (4) is reduced to the OVM [11]. When $\tau_1 = \tau_2$, (4) degenerates to the car-following model considering self-stabilizing control in historical traffic data [21].

For the convenience of stability analysis, we transform (4) into the following form:

$$\begin{cases} \dfrac{dv_n(t)}{dt} = \alpha\left[V\left(\Delta x_n(t)\right) - v_n(t)\right] + \tilde{u}_n(t-\tau_1) \\ \qquad\qquad + \tilde{e}_n(t-\tau_2) \\ \dfrac{dx_n(t)}{dt} = v_n(t) \end{cases} \tag{8}$$

III. STABILITY ANALYSIS OF THE CONTROLLED OVM

In this section, the stability analysis of the OVM with double time-delayed feedback control is executed to investigate the characteristics of bifurcation. Assume that N vehicles drive on a single-track circular road with a length of L without overtaking. Thereby uniform flow can be described as all vehicles travel at the desired speed and maintain the same headway, whose corresponding equilibrium solution is shown as follows:

$$\begin{aligned} v_n^0(t) &= V\left(h^*\right), \quad \Delta x_n(t) = h^* = \frac{L}{N}, \\ x_n^0(t) &= nh^* + V\left(h^*\right)t \end{aligned} \tag{9}$$

Adding a small derivation to the uniform flow (9):

$$v_n^0(t) = V\left(h^*\right) + \eta_n(t), \quad x_n^0(t) = nh^* + V\left(h^*\right)t + \xi_n(t) \tag{10}$$

where $\eta_n(t)$ and $\xi_n(t)$ denote derivation.

By inserting (10) into (8) and linearizing yields:

$$\begin{cases} \dfrac{d\eta_n(t)}{dt} = \beta\left(\xi_{n+1}(t) - \xi_n(t)\right) + \varepsilon\eta_n(t) - \gamma_1\eta_n(t-\tau_1) \\ \qquad\qquad - \delta\left(\xi_{n+1}(t-\tau_2) - \xi_n(t-\tau_2)\right) \\ \dfrac{d\xi_n(t)}{dt} = \eta_n(t) \end{cases} \tag{11}$$

where $\beta = (\alpha + \gamma_2)V'$, $\varepsilon = (\gamma_1 - \alpha)$ and $\delta = \gamma_2 V'$; $V'(h^*)$ is abbreviated as V'; the subscript $n \in \{1, 2, \cdots N\}$ indicates the vehicle number.

Considering the periodic boundary, (11) be simplified into matrix form:

$$\begin{aligned} \begin{pmatrix} \dot{\eta} \\ \dot{\xi} \end{pmatrix} &= \begin{pmatrix} \varepsilon\mathbf{I} & -\beta\mathbf{A} \\ \mathbf{I} & \mathbf{O} \end{pmatrix}\begin{pmatrix} \eta \\ \xi \end{pmatrix} + \begin{pmatrix} -\gamma_1\mathbf{I} & \mathbf{O} \\ \mathbf{O} & \mathbf{O} \end{pmatrix}\begin{pmatrix} \eta(t-\tau_1) \\ \xi(t-\tau_1) \end{pmatrix} \\ &\quad + \begin{pmatrix} \mathbf{O} & \delta\mathbf{A} \\ \mathbf{O} & \mathbf{O} \end{pmatrix}\begin{pmatrix} \eta(t-\tau_2) \\ \xi(t-\tau_2) \end{pmatrix} \end{aligned} \tag{12}$$

where $\eta = (\eta_1(t), \eta_2(t), \cdots, \eta_N(t))^T$, $\xi = (\xi_1(t), \xi_2(t), \cdots, \xi_N(t))^T$; $\mathbf{O}$ is the zero matrix of $N \times N$. The form of Matrix $\mathbf{A}$ is as follows:

$$\mathbf{A} = \begin{pmatrix} 1 & -1 & 0 & \cdots & 0 & 0 \\ 0 & 1 & -1 & \cdots & 0 & 0 \\ \vdots & \vdots & \vdots & & \vdots & \vdots \\ 0 & 0 & 0 & \cdots & 1 & -1 \\ -1 & 0 & 0 & \cdots & 0 & 1 \end{pmatrix} \tag{13}$$

The corresponding characteristic equation of (12) can be derived as follows:

$$\left[\lambda^2 - \varepsilon\lambda + \gamma_1 e^{-\tau_1\lambda}\lambda + \beta - \delta e^{-\tau_2\lambda}\right]^N - \left[\beta - \delta e^{-\tau_2\lambda}\right]^N = 0 \tag{14}$$

(14) is equivalent to the following one:

$$\left[\frac{\lambda^2 - \varepsilon\lambda + \gamma_1 e^{-\tau_1\lambda}\lambda + \beta - \delta e^{-\tau_2\lambda}}{\beta - \delta e^{-\tau_2\lambda}}\right]^N = 1 \tag{15}$$

Solving (15) yields:

$$\begin{aligned} \lambda^2 - \varepsilon\lambda + \gamma_1 e^{-\tau_1\lambda}\lambda + \beta - \delta e^{-\tau_2\lambda} &= \left(\beta - \delta e^{-\tau_2\lambda}\right) \\ &\quad \times \left(\cos\frac{2k\pi}{N} + i\sin\frac{2k\pi}{N}\right) \end{aligned} \tag{16}$$

where $k \in \{1, 2, \cdots N\}$ is wave number representing the oscillation mode.

Inserting $\lambda = \mu + i\omega$ (where μ and ω are real and imaginary part of λ, respectively; i is an imaginary unit) into (16) and separating the real and imaginary parts yield:

$$\begin{cases} \mu^2 - \omega^2 - \varepsilon\mu + \gamma_1 e^{-\tau_1\mu}\left(\mu c_{\tau 1} + \omega s_{\tau 1}\right) + \beta \\ \quad - \delta e^{-\tau_2\mu}c_{\tau 2} = \beta c_k - \delta e^{-\tau_2\mu}c_{\tau 2}c_k - \delta e^{-\tau_2\mu}s_{\tau 2}s_k \\ 2\mu\omega - \varepsilon\omega + \gamma_1 e^{-\tau_1\mu}\left(\omega c_{\tau 1} - \mu s_{\tau 1}\right) + \delta e^{-\tau_2\mu}s_{\tau 2} \\ \quad = \beta s_k - \delta e^{-\tau_2\mu}c_{\tau 2}s_k + \delta e^{-\tau_2\mu}s_{\tau 2}c_k \end{cases} \tag{17}$$

where $c_k = \cos(2k\pi/N)$, $s_k = \sin(2k\pi/N)$, $c_{\tau 1} = \cos\tau_1\omega$, $c_{\tau 2} = \cos\tau_2\omega$, $s_{\tau 1} = \sin\tau_1\omega$, $s_{\tau 2} = \sin\tau_2\omega$.

If $k = N$ in the (17), the following formula holds:

$$\left[\mu^2 - \omega^2 - \varepsilon\mu\right]^2 + [2\mu\omega - \varepsilon\omega]^2 = \left(\mu^2 + \omega^2\right)\gamma_1^2 e^{-2\mu\tau_1} \tag{18}$$

Obviously, for $k = N$, (18) with μ and ω as dependent variables and V' as independent variable has two roots, one is $(0, 0)$, and the other is $(f, 0)$, where the value of f depends on γ_1, τ_1 and ε (i.e. $\gamma_1 - \alpha$). In other words, with V' increasing, the eigenvalue always shows two fixed points in the coordinate area, one is located at $(0, 0)$ and the other is located at $(f, 0)$ for $k = N$. For fixed $N = 7$ and every $k \neq N$, the real and imaginary part distributions of eigenvalues for (16) are shown in the Fig. 2. Fig. 2(a) depicts the distribution of eigenvalues of uncontrolled OVM, namely, $\gamma_1 = 0$, $\gamma_2 = 0$. When $V' = 0$, the eigenvalues are located at $(0, 0)$ and $(-1, 0)$ for each k. Then, as V' increases, the eigenvalues of different k separate from $(0, 0)$ and $(-1, 0)$ along the corresponding hyperbolic trajectory. For a sufficiently small $V' > 0$, the eigenvalues for every k are all located on the left half of the complex plane, which indicates that the system is asymptotic stable [16]. However, when V' is large enough, the eigenvalues cross the imaginary axis, and the system suddenly loses stability, where the point on the imaginary axis is the critical point called the Hopf bifurcation point. From Fig. 2(a), we notice that the eigenvalues corresponding to $k = 1$ and $k = 6$ first cross the imaginary axis, then $k = 2$ and $k = 5$, and finally $k = 3$ and $k = 4$ which take more time to cross the imaginary axis. What reveals in Fig. 2(b) is the eigenvalue distribution of the controlled OVM. In Fig. 2(b), for $k = 1$, the length of hyperbolic trajectory in the left half complex plane is longer than that in Fig. 2(a). Moreover, for $k = 3$, the trajectory moves to the left in the opposite trend as shown in Fig. 2(a). In this way, the whole trajectory corresponding to $k = 3$ is in the left half complex plane, which demonstrates that the controlled OVM can suppress or defer the occurrence of Hopf bifurcation. It further illustrates that a reasonable delay design can postpone or eliminate the impact of Hopf bifurcation.

It can be seen from Fig. 2 that when the eigenvalue crosses the imaginary axis, the stability will change dramatically. That is to say, when a pair of pure imaginary roots $\lambda_{1,2} = \pm i\omega$ appear in the system, the Hopf bifurcation will occur. Therefore, introducing $\lambda = i\omega$ into (16), the critical condition for Hopf bifurcation yields:

$$\begin{cases} -\omega^2 + \gamma_1\omega s_{\tau 1} + \beta - \delta c_{\tau 2} = \beta c_k - \delta c_{\tau 2} c_k - \delta s_{\tau 2} s_k \\ -\varepsilon\omega + \gamma_1\omega c_{\tau 1} + \delta s_{\tau 2} = \beta s_k - \delta c_{\tau 2} s_k + \delta s_{\tau 2} c_k \end{cases} \tag{19}$$

Let $\gamma_1 = 0$ and $\gamma_2 = 0$ in (19), the stability condition (19) can be simplified as follows:

$$\alpha = 2\cos^2\left(\frac{k\pi}{N}\right) V' \tag{20}$$

Obviously, (20) can be further reduced to $\alpha > 2V'$, which is identical with the stability condition of uncontrolled OVM in Ref. [11]. Therefore, when $\alpha < 2V'$ holds, uniform traffic flow will evolve into a stagnant traffic for the uncontrolled OVM.

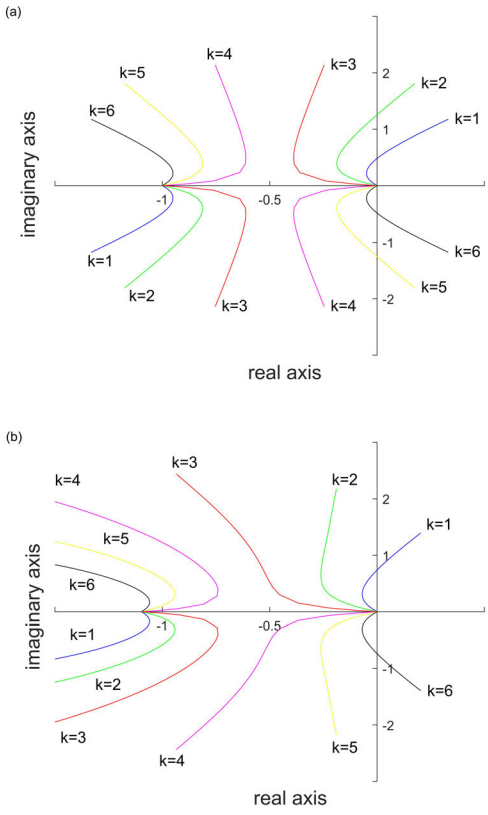

FIGURE 2. Eigenvalues of the system for $a = 1\ s^{-1}$ and $N = 7$: (a) uncontrolled OVM with $\gamma_1 = 0$ and $\gamma_2 = 0$; (b) controlled OVM with $\gamma_1 = 0.4\ s^{-1}$, $\gamma_2 = 0.7\ s^{-1}$, $\tau_1 = 0.2$ s and $\tau_2 = 0.3$ s.

Subsequently, linear stable curves are shown in Fig. 3 by solving the (19) of headway h^* and sensitivity α. Note that the upper area of the curve in Fig. 3 is the stable region, and the lower is the unstable region. In Fig. 3, the blue line represents the uncontrolled OVM, and the other four colorful lines represent four different combinations of time-delayed feedback control strategies. For Fig. 3(a), multiple sets of time-delayed parameters are selected with fixed feedback coefficients (i.e. $\gamma_1 = 0.25\ s^{-1}$, $\gamma_2 = 0.25\ s^{-1}$). Obviously, as τ_2 increases, the stable region increases with fixed $\tau_1 = 0.7$ s, and the control effect with the parameter set to $\gamma_1 = 0.7\ s^{-1}$ and $\gamma_2 = 0.9\ s^{-1}$ is the best. However, in Fig. 3, when we retain the time-delay parameter invariant and alter the feedback coefficient $\gamma_1 = 0.75\ s^{-1}$ and $\gamma_2 = 0.75\ s^{-1}$, an interesting phenomenon will appear. The stability region expands gradually with τ_2 increasing from 0.1 to 0.4, while the stable region shrinks with τ_2 increasing from 0.4 to 0.9, which is different from the trend in Fig. 3(a). Similarly, in Fig. 3(c), multiple sets of feedback coefficients are chosen with fixed time-delayed parameters (i.e. $\tau_1 = 1.5$ s, $\tau_2 = 0.5$ s). For fixed $\gamma_1 = 0.3\ s^{-1}$, the stable region expands with γ_2 increasing. Conversely, when selecting $\tau_1 = 1$ s and $\tau_2 = 1.25$ s, the stable region decreases as γ_2 increases in Fig. 3(d).

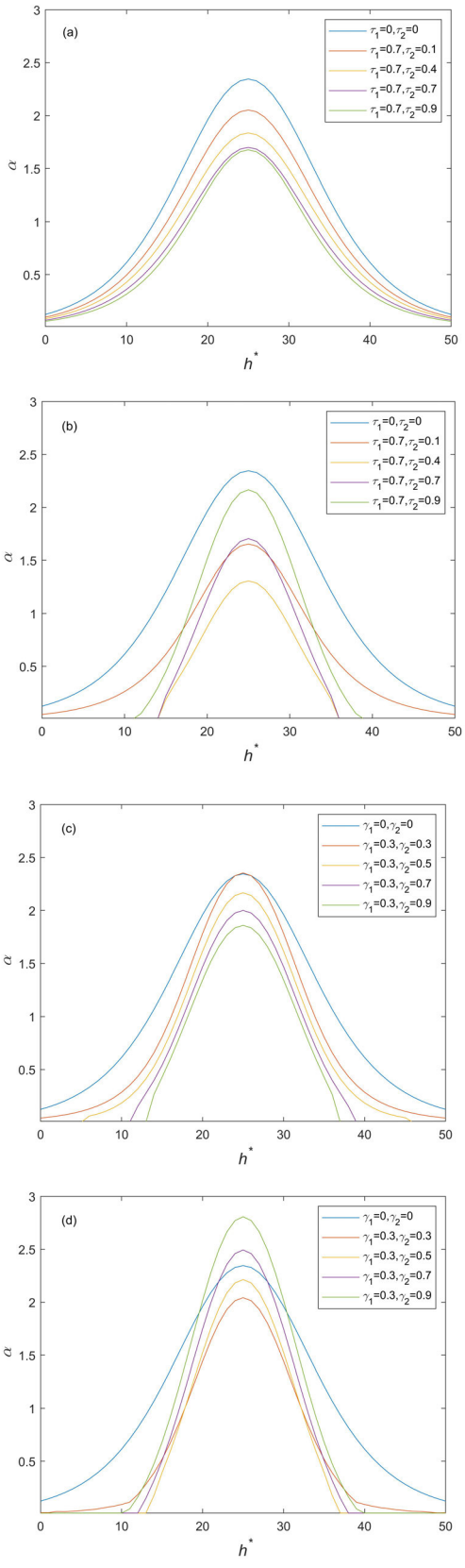

FIGURE 3. Stability diagram of the system (4) in the (h^*, α) plane for $k = 1$ and $N = 7$ with fixed: (a) $\gamma_1 = 0.25\,\mathrm{s}^{-1}$, $\gamma_2 = 0.25\,\mathrm{s}^{-1}$; (b) $\gamma_1 = 0.75\,\mathrm{s}^{-1}$, $\gamma_2 = 0.75\,\mathrm{s}^{-1}$; (c) $\tau_1 = 1.5\,\mathrm{s}$, $\tau_2 = 0.5\,\mathrm{s}$; (d) $\tau_1 = 1\,\mathrm{s}$, $\tau_2 = 1.25\,\mathrm{s}$.

Moreover, the vertices of the green and purple curves representing the controlled OVM in Fig. 3(d) are higher than that of the blue curve representing the uncontrolled OVM, which means that the two control strategies represented by green and purple curves cannot suppress the oscillation well. In general, Fig. 3 demonstrates that there is no single linear relationship between parameter values and stability. Therefore, in the design of time-delayed control, it is important to select appropriate control parameters by leveraging reasonable methods to stabilize traffic flow. In the next section, we will discuss the design of time-delayed feedback control in detail.

IV. THE DESIGN OF DOUBLE TIME-DELAY FEEDBACK CONTROL

The design of time-delay control for nonlinear systems is an issue worth studying [22]–[25]. From Section 3, it is obvious that reasonable parameter setting can postpone the occurrence of bifurcation or reduce the negative effect of bifurcation. Hence, in Section 4, an improved definite integral method proposed by Xu *et al.* [26] is utilized to select the appropriate combination of time-delayed parameters and feedback coefficients, so as to design a reasonable double time-delay feedback control strategy to contain bifurcation behavior in OVM. The following characteristic equation from (16) is indispensable to the stability method:

$$f(\lambda) = \lambda^2 - \varepsilon\lambda + \gamma_1 e^{-\tau_1\lambda}\lambda + \beta - \delta e^{-\tau_2\lambda} - \left(\beta - \delta e^{-\tau_2\lambda}\right) \times \left(\cos\frac{2k\pi}{N} + i\sin\frac{2k\pi}{N}\right) \quad (21)$$

Generally, the time-delayed control strategy is designed by the Nyquist criterion [27], since it can judge stability well in case of a single delay, while for the case of multiple delays, it works ineffectively. Therefore, a definite integral method was proposed by Kolmanovskii and Myshkis [28] to address the issue. The core of the method is to calculate a definite integral whose integrand is a transcendental real equation related to the characteristic equation. The result calculated by the definite integral represents the number Ω of characteristic roots in the right-half complex plane. If $\Omega = 0$, the controlled system (4) will be stable for the selected time-delayed parameters and feedback coefficients. Otherwise $\Omega \neq 0$, the system is in an unstable state, and stop-and-go wave appears in the traffic flow. The issue of multiple time-delayed control design seems to be well solved. However, there is a defect in this method, that is, there is no general rule for estimating the upper limit of definite integral. Thereby Xu *et al.* [26] added an ingenious and tractable algorithm into the definite integral method whose function is choosing the upper limit of integral. The specific procedure of the improved definite integral method is given in Appendix.

In order to facilitate readers to better understand the operation process of the above steps, an example is implemented to illustrate how to determine the stability of the system for $\alpha = 2\ \mathrm{s}^{-1}$, $V' = 1.448$, $\gamma_1 = 0.3\ \mathrm{s}^{-1}$ and $\gamma_2 = 0.5\ \mathrm{s}^{-1}$. Select the time-delayed parameters as $(\tau_1, \tau_2) = (1.25, 1.5)$ and insert them into (A1), and then the maximum positive

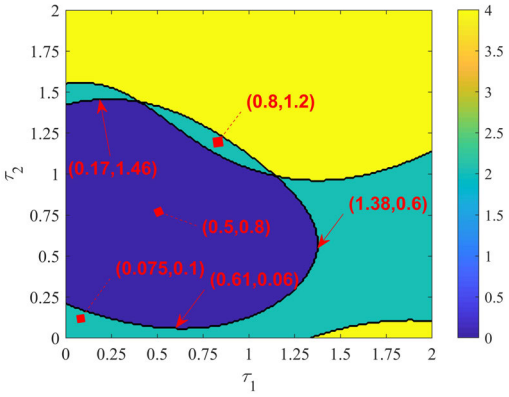

FIGURE 4. The stability chart of the controlled OVM with regard to τ_1 and τ_2 for $\gamma_1 = 0.3\ \mathrm{s}^{-1}$, $\gamma_2 = 0.5\ \mathrm{s}^{-1}$ and $\alpha = 2\ \mathrm{s}^{-1}$.

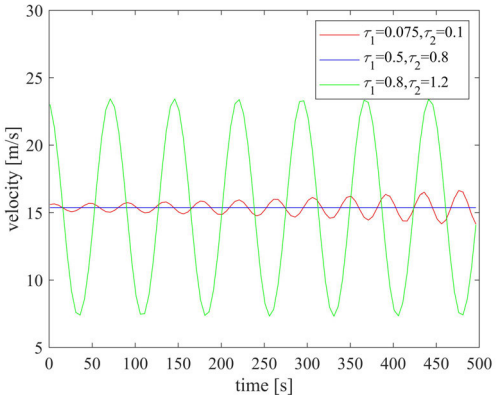

FIGURE 5. Time evolution of velocity for the first vehicle with different time-delayed parameters combinations in Fig. 4 and $\alpha = 2\ \mathrm{s}^{-1}$, $\gamma_1 = 0.3\ \mathrm{s}^{-1}$ and $\gamma_2 = 0.5\ \mathrm{s}^{-1}$.

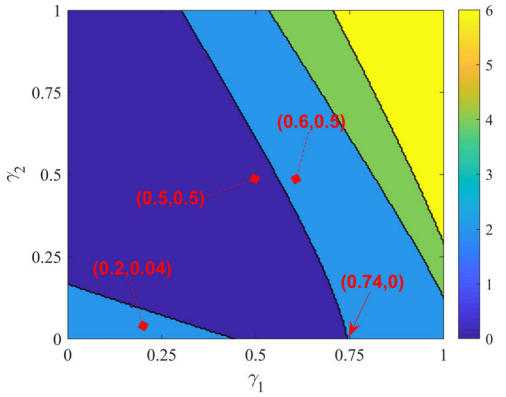

FIGURE 6. The stability chart of the controlled OVM with regard to γ_1 and γ_2 for $\tau_1 = 0.7$ s, $\tau_2 = 0.9$ s and $\alpha = 2\ \mathrm{s}^{-1}$.

root of $R(\omega) = 0$ can be obtained as $\omega_{\max} = 1.5481$ for $k = 1$. Selecting $T_0 = 1.6481 > \omega_{\max}$ as the upper limit of definite integral, (A7) can yield that $F(0, T_0)_{k=1}$. Further, (A8) yields that $\Omega_{k=1}(\tau_1, \tau_2) = 1$. Repeating the above calculation process, $\Omega_{k=2,5,6}(\tau_1, \tau_2) = 1$ and $\Omega_{k=3,4}(\tau_1, \tau_2) = 0$ are figured out. Adding up all characteristic roots in the right-half complex plane, $\Omega(1.25, 1.5) = \sum_{k=1}^{N-1} \Omega_k(1.25, 1.5) = 4$ can be obtained, which indicates that the system for $(\gamma_1, \gamma_2, \tau_1, \tau_2) = (0.3, 0.5, 1.25, 1.5)$ is unstable.

Subsequently, the above steps will be executed to judge the stability of the system (4) for different parameter combinations. The common parameters such as headway h^*, derivative of optimal speed function (7) related to headway $V'(h^*)$ and the number of vehicles N are set as follows:

$$\Delta x_n(t) = h^* = 25\ \mathrm{m}, \quad V' = V'\left(h^*\right) = 1.448,\ N = 7 \tag{22}$$

Note that $\alpha = 2\ \mathrm{s}^{-1} < 2V'$ corresponding to the uncontrolled OVM of unstable state is selected in the following simulation for the purpose of reflecting the control performance of our designed double time-delay feedback control strategy.

Fig. 4 shows the stability of the controlled OVM for $\gamma_1 = 0.3\ \mathrm{s}^{-1}$ and $\gamma_2 = 0.5\ \mathrm{s}^{-1}$ in $(\tau_1, \tau_2) \in [0, 2] \times [0, 2]$. In Fig. 4, the dark blue region representing $\Omega(\tau_1, \tau_2) = 0$ is the stable region; the green region representing $\Omega(\tau_1, \tau_2) = 2$ and the yellow region representing $\Omega(\tau_1, \tau_2) = 4$ are the unstable region. From Fig. 4, when $\tau_1 \in [0, 1.38]$, there always exists appropriate τ_2 to make the system stable, while for $\tau_1 \in (1.38, 2]$, the system is unstable regardless of the value of τ_2. Similarly, when $\tau_2 \in [0.06, 1.46]$, appropriate τ_1 always presents to stabilize the system, otherwise the system is unstable. For the sake of validating control effect, several sets of parameter combinations in Fig. 4 are chosen to describe the velocity fluctuation of the first vehicle under the corresponding parameter conditions, as shown in Fig. 5. From Fig. 5, when $(\gamma_1, \gamma_2, \tau_1, \tau_2) = (0.3, 0.5, 0.5, 0.8)$ represented by the blue line which is located in the stable region in Fig. 3, the velocity has been maintained at a constant value over time, which strictly conforms to the property of stable traffic flow. When $(\gamma_1, \gamma_2, \tau_1, \tau_2) = (0.3, 0.5, 0.075, 0.1)$ and $(\gamma_1, \gamma_2, \tau_1, \tau_2) = (0.3, 0.5, 0.8, 1.2)$ which are located in the unstable region, the velocity represented by the green line oscillates at a constant amplitude, and the velocity represented by the red line increases in amplitude over time, which are consistent with the behaviors of unstable traffic flow.

Analogous to the time-delayed parameter design mentioned above, the feedback coefficients design is shown in Fig. 6. What reveals in Fig. 6 is the stability chart of controlled OVM for $\tau_1 = 0.7$ s and $\tau_2 = 0.9$ s in $(\gamma_1, \gamma_2) \in [0, 1] \times [0, 1]$. In Fig. 6, the stable area is shown in navy blue for $\Omega(\tau_1, \tau_2) = 0$, and there are three unstable areas: light blue ($\Omega(\tau_1, \tau_2) = 2$), green ($\Omega(\tau_1, \tau_2) = 4$) and yellow ($\Omega(\tau_1, \tau_2) = 6$). For $\gamma_1 \in [0, 0.74]$, there always exists a suitable γ_2 to suppress the traffic fluctuation, while for $\gamma_1 \in (0.74, 1]$, the oscillation generated by the uncontrolled OVM will not be alleviated, regardless of the value of γ_2. In the same way, for arbitrary γ_2, there is always a certain interval of γ_1 to restrain the original stop-and-go wave.

In Fig. 7, several sets of parameters in Fig. 6 are selected to verify the rationality of the control strategy through time-velocity evolution for the first vehicle. For

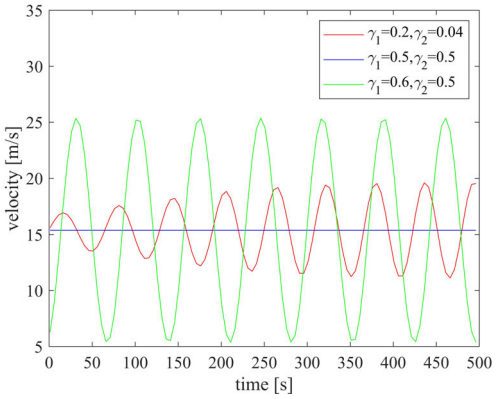

FIGURE 7. Time evolution of velocity for the first vehicle with different feedback coefficients combinations in Fig. 6 and $\tau_1 = 0.7$ s, $\tau_2 = 0.9$ s and $\alpha = 2\ s^{-1}$.

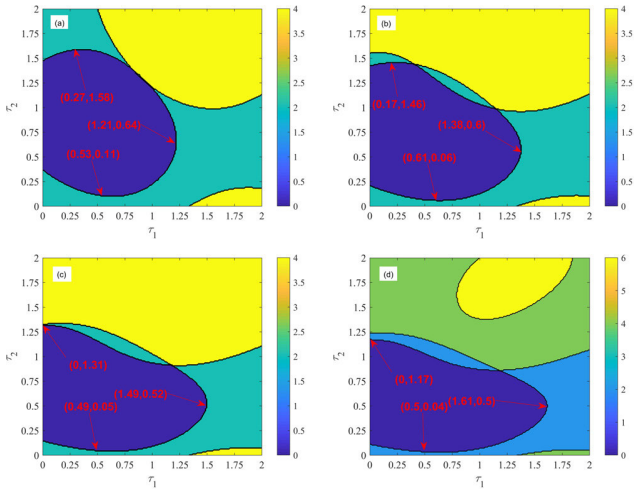

FIGURE 8. The stability chart of the controlled OVM with regard to τ_1 and τ_2 for $\alpha = 2\ s^{-1}$, $\gamma_1 = 0.3\ s^{-1}$ and: (a) $\gamma_2 = 0.3\ s^{-1}$; (b) $\gamma_2 = 0.5\ s^{-1}$; (c) $\gamma_2 = 0.7\ s^{-1}$; (d) $\gamma_2 = 0.9\ s^{-1}$.

$(\gamma_1, \gamma_2, \tau_1, \tau_2) = (0.5, 0.5, 0.7, 0.9)$ in the stable region, the corresponding blue line has been kept horizontal, which means that the unstable traffic flow grown by uncontrolled OVM is contained. On the contrary, when the parameter combination is not contained in the stable region, such as $(\gamma_1, \gamma_2, \tau_1, \tau_2) = (0.2, 0.04, 0.7, 0.9)$ and $(\gamma_1, \gamma_2, \tau_1, \tau_2) = (0.6, 0.5, 0.7, 0.9)$, the red and green lines they represent both show sharp fluctuations in velocity.

Fig. 8-11 are simulated to observe how the stable region changes when a certain control parameter varies. In Fig. 8, for fixed $\gamma_1 = 0.3\ s^{-1}$ and with the increase of γ_2, the length of optional stable interval for τ_2 decreases from 1.47 to 1.13, while that of τ_1 increases from 1.21 to 1.61. Conversely, when fixing $\gamma_2 = 0.5\ s^{-1}$ and increasing γ_1, the length of optional stable interval for τ_2 raises from 1.29 to 1.49, and that of τ_1 reduces from 2 to 0.83, as shown in Fig. 9. From Fig. 10, for fixed $\tau_1 = 0.7$ s, when τ_2 raises from 0.1 to 0.4, the area of stable region in γ_1 and γ_2 expands, while for τ_2 increasing from 0.4 to 0.9, the area of that narrows gradually. There is

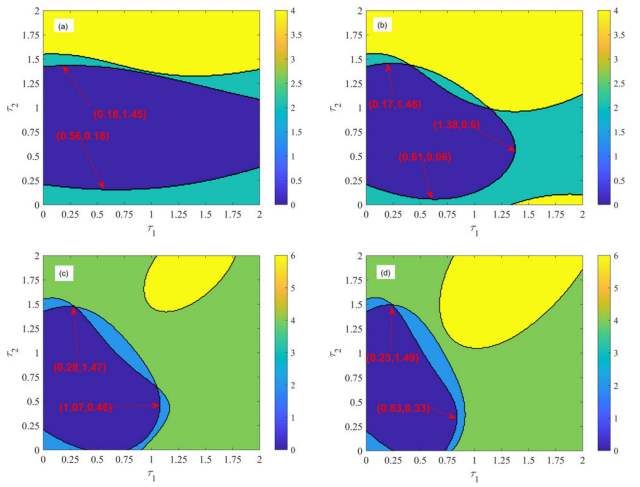

FIGURE 9. The stability chart of the controlled OVM with regard to τ_1 and τ_2 for $\alpha = 2\ s^{-1}$, $\gamma_2 = 0.5\ s^{-1}$ and: (a) $\gamma_1 = 0.1\ s^{-1}$; (b) $\gamma_1 = 0.3\ s^{-1}$; (c) $\gamma_1 = 0.5\ s^{-1}$; (d) $\gamma_1 = 0.7\ s^{-1}$.

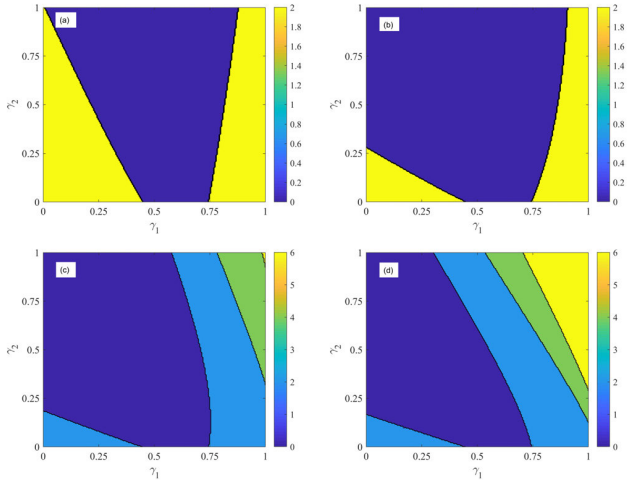

FIGURE 10. The stability chart of the controlled OVM with regard to γ_1 and γ_2 for $\alpha = 2\ s^{-1}$, $\tau_1 = 0.7$ s and: (a) $\tau_2 = 0.1$ s; (b) $\tau_2 = 0.4$ s; (c) $\tau_2 = 0.7$ s; (d) $\tau_2 = 0.9$ s.

a similar trend between Fig. 10 and Fig. 11. In Fig. 11, for fixed $\tau_2 = 0.7$ s, the area of stable region with respect to γ_1 and γ_2 firstly ascends and then descends with the adding of τ_1.

According to the simulation and analysis of Fig. 4-11, the feasibility of the improved definite integral stability method in traffic flow model is verified, which lays the foundation for the following study.

V. CASE STUDIES

A. CASE 1

In order to further verify the effectiveness of the design for double time-delay control, the number of simulated vehicles N is increased to 100, which approximates the operation of actual traffic. Assume that the initial state is N vehicles traveling on a 2000 m long circular road with identical speed

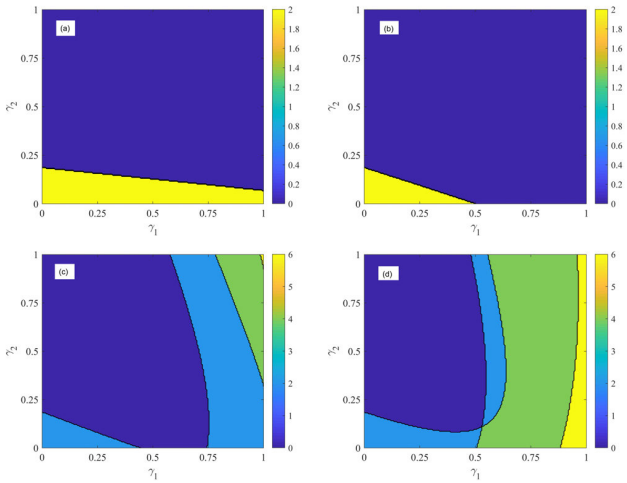

FIGURE 11. The stability chart of the controlled OVM with regard to γ_1 and γ_2 for $\alpha = 2\ \mathrm{s}^{-1}$, $\tau_2 = 0.7$ s and: (a) $\tau_1 = 0.1$ s; (b) $\tau_1 = 0.4$ s; (c) $\tau_1 = 0.7$ s; (d) $\tau_1 = 0.9$ s.

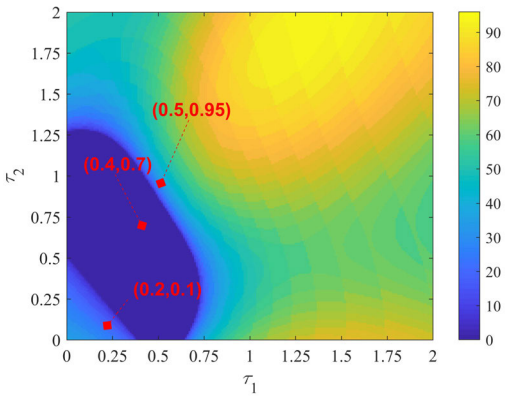

FIGURE 12. The stability chart of the controlled OVM with regard to τ_1 and τ_2 for $\gamma_1 = 0.8\ \mathrm{s}^{-1}$, $\gamma_2 = 0.6\ \mathrm{s}^{-1}$ and $\alpha = 2\ \mathrm{s}^{-1}$.

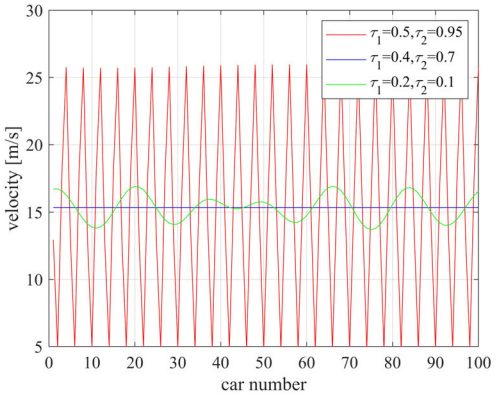

FIGURE 13. Time evolution of velocity for all vehicles at $t = 2000$ s with different time-delayed parameters combinations in Fig. 12 and $\gamma_1 = 0.8\ \mathrm{s}^{-1}$, $\gamma_2 = 0.6\ \mathrm{s}^{-1}$ and $\alpha = 2\ \mathrm{s}^{-1}$.

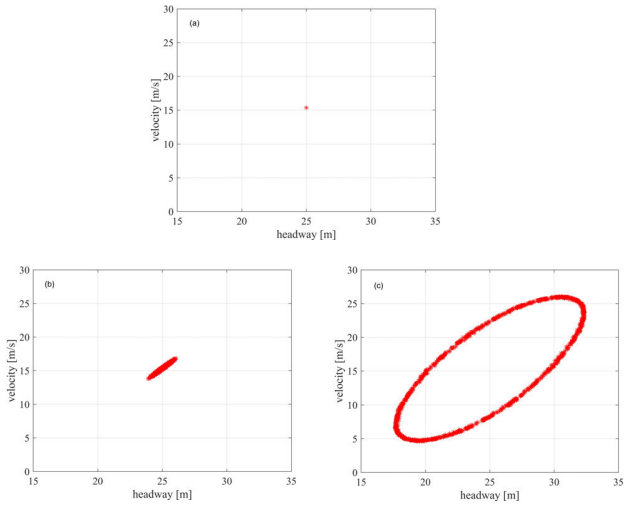

FIGURE 14. The hysteresis loops for the controlled OVM correspond to Fig. 13.

and distance, and the mathematical expression is as follows:

$$x_n(0) = nh^* + y_n(0), \quad v_n(0) = V\left(h^*\right), \ h^* = \frac{L}{N} \tag{23}$$

where $y_n(0)$ is a random perturbation with an amplitude of 0.01.

For fixed $\gamma_1 = 0.8\ \mathrm{s}^{-1}$, $\gamma_2 = 0.6\ \mathrm{s}^{-1}$ and $\alpha = 2\ \mathrm{s}^{-1}$ corresponding to the unstable OVM, the stable region of the controlled OVM is determined in $(\tau_1, \tau_2) \in [0, 2] \times [0, 2]$, as shown in Fig. 12. The dark blue area at the bottom left of Fig. 12 is a stable region (i.e. $\Omega(\tau_1, \tau_2) = 0$), and the rest are unstable region (i.e. $\Omega(\tau_1, \tau_2) \neq 0$). Then, select arbitrary three point, for example, $(\tau_1, \tau_2) = (0.4, 0.7)$ from the stable region, $(\tau_1, \tau_2) = (0.2, 0.1)$ and $(\tau_1, \tau_2) = (0.5, 0.95)$ from the unstable region. It can be seen from Fig. 13 that the blue line representing $(\tau_1, \tau_2) = (0.4, 0.7)$ remains horizontal at $t = 2000$ s, which indicates that all vehicles travel at velocity $V(h^*)$ and this set of control parameters $(\gamma_1, \gamma_2, \tau_1, \tau_2) = (0.8, 0.6, 0.4, 0.7)$ can effectively decay traffic fluctuation. While the value of velocity of the other two lines in Fig. 13 still fluctuate in different degrees, which demonstrates that these two sets of control parameters have negative control effect on the speed fluctuation.

The hysteresis loop is an important reason for the instability and stagnation of traffic flow. In addition, the stronger the hysteresis effect, the greater the disturbance to the steady traffic flow. In Fig. 14, the hysteresis loop for $(\tau_1, \tau_2) = (0.4, 0.7)$ is reduced to a point compared with $(\tau_1, \tau_2) = (0.2, 0.1)$ and $(\tau_1, \tau_2) = (0.5, 0.95)$, which is also consistent with the stability shown in Fig. 12.

To better compare the uncontrolled OVM with the controlled OVM with $(\gamma_1, \gamma_2, \tau_1, \tau_2) = (0.8, 0.6, 0.4, 0.7)$, Fig. 15 and Fig. 16 are plotted. The dynamic behavior of the uncontrolled OVM is shown in Fig. 15(a) and 16(a) where irregular stop-and-go waves appear in the traffic flow, which is in sharp contrast with the controlled OVM in Fig. 15(b) and 16(b) where traffic flow is homogeneous.

Subsequently, with $\tau_1 = 0.5$ s, $\tau_2 = 0.8$ s and $\alpha = 2\ \mathrm{s}^{-1}$ fixed, the stability chart for γ_1 and γ_2 is plotted, as shown in

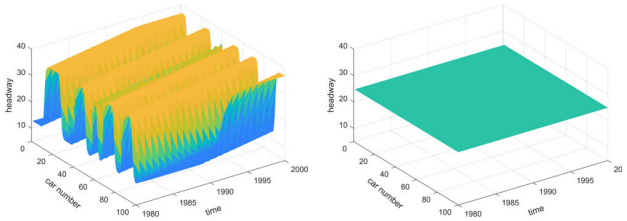

(a) Uncontrolled OVM (b) Controlled OVM

FIGURE 15. Comparison between the uncontrolled OVM (i.e. $\tau_1 = 0$ and $\tau_2 = 0$) and the controlled OVM (i.e. $\tau_1 = 0.4$ s and $\tau_2 = 0.7$ s) with fixed $\gamma_1 = 0.8\ \mathrm{s}^{-1}$, $\gamma_2 = 0.6\ \mathrm{s}^{-1}$ and $\alpha = 2\ \mathrm{s}^{-1}$.

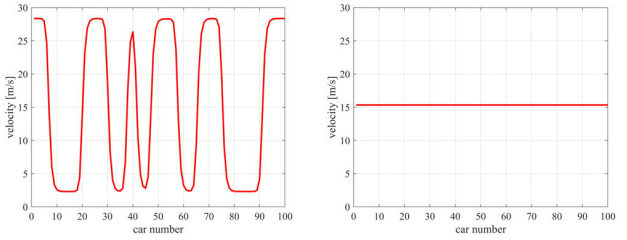

(a) Uncontrolled OVM (b) Controlled OVM

FIGURE 16. The snapshots of velocity for all vehicles at $t = 2000$ s correspond to Fig. 15.

Fig. 17. In Fig. 17, the stable region is colored in dark blue, where the appropriate combination of control parameters will come from, while the rest is the unstable region. In Fig. 18, three sets control parameters from Fig. 17 are chosen to observe their velocity evolution over time. Obviously, the blue line representing $(\gamma_1, \gamma_2) = (0.75, 0.5)$ in stable region always stays at the optimal velocity $V(h^*)$. While the red line and green line represented by $(\gamma_1, \gamma_2) = (0.16, 0.15)$ and $(\gamma_1, \gamma_2) = (0.875, 0.725)$ appear irregular oscillation. Moreover, the hysteresis loops in Fig. 19 corresponding to Fig. 18 shows the same trend as Fig. 18, that is, the more stable, the smaller the hysteresis loop. For example, the most stable $(\gamma_1, \gamma_2) = (0.75, 0.5)$ whose delay loop is reduced to a point.

For the sake of verifying the control effect of the selected control parameters combination $(\gamma_1, \gamma_2, \tau_1, \tau_2) = (0.75, 0.5, 0.5, 0.8)$, comparison between the uncontrolled and controlled OVM is shown in Fig. 20 and 21. In Fig. 20(a) and Fig. 21(a), the uncontrolled OVM results in frequent traffic stagnation and obvious velocity fluctuations. However, when we apply a double time-delay control to the uncontrolled OVM, the stop-and-go wave decays and the traffic flow returns to stability, which indicates the effectiveness of the double time-delay control strategy.

B. CASE 2

1) DATA SOURCES

In this section, we utilize the vehicle trajectory real data from the NGSIM project of the Federal Highway Administration of USA which is an open data source to calibrate the parameters

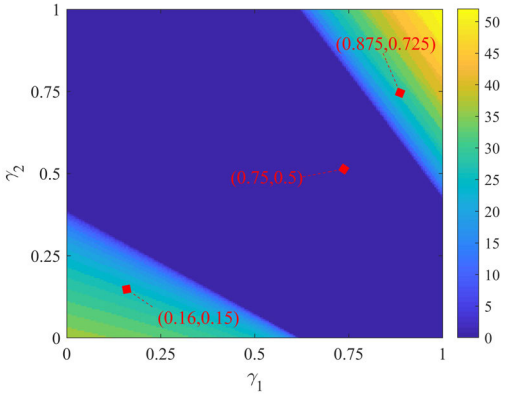

FIGURE 17. The stability chart of the controlled OVM with regard to γ_1 and γ_2 for $\tau_1 = 0.5$ s, $\tau_2 = 0.8$ s and $\alpha = 2\ \mathrm{s}^{-1}$.

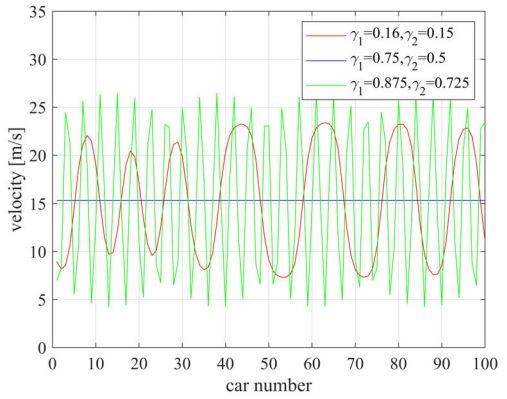

FIGURE 18. Time evolution of velocity for all vehicles at $t = 2000$ s with different time-delayed parameters combinations in Fig. 17 and $\tau_1 = 0.5$ s, $\tau_2 = 0.8$ s and $\alpha = 2\ \mathrm{s}^{-1}$.

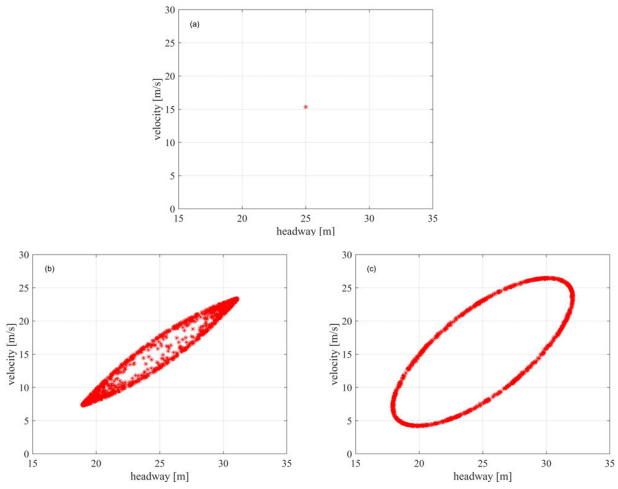

FIGURE 19. The hysteresis loops for the controlled OVM correspond to Fig. 18.

of the model, so as to verify the effect of double time-delay control. The data were collected on freeway 101 in Los Angeles, California, including the acceleration, speed and location of each vehicle on multiple lanes. According

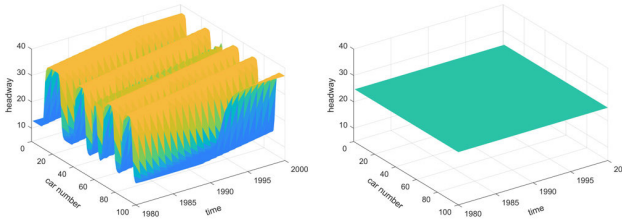

(a) Uncontrolled OVM (b) Controlled OVM

FIGURE 20. Comparison between the uncontrolled OVM (i.e. $\gamma_1 = 0$ and $\gamma_2 = 0$) and the controlled OVM (i.e. $\gamma_1 = 0.75\ \mathrm{s}^{-1}$ and $\gamma_2 = 0.5\ \mathrm{s}^{-1}$) with fixed $\tau_1 = 0.5$ s, $\tau_2 = 0.8$ s and $\alpha = 2\ \mathrm{s}^{-1}$.

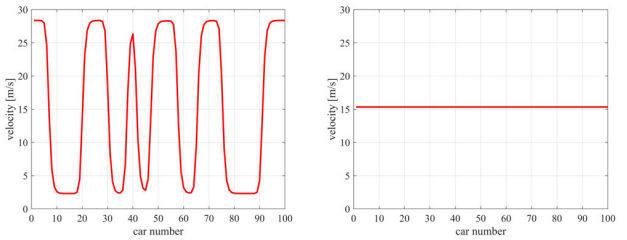

(a) Uncontrolled OVM (b) Controlled OVM

FIGURE 21. The snapshots of velocity for all vehicles at correspond to Fig. 20.

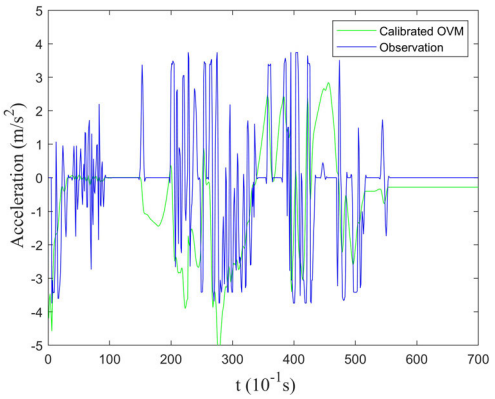

FIGURE 22. Observed and simulated acceleration curves.

to the data screening criteria in Ref. [29], the trajectory data are filtered and processed, and two sets of qualified data are obtained, which are recorded as dataset A and dataset B. Dataset A contains 709 sets of data to calibrate the model and dataset B contains 668 sets of data to verify the parameters after calibration.

2) PARAMETER CALIBRATION METHOD

At present, many methods have been applied in the process of calibration, including least square method [30], maximum likelihood method [31], genetic algorithm [32], monkey algorithm [33] and so on, among which genetic algorithm (GA) is the most widely used. Genetic algorithm is a method of simulating natural selection and genetic theory in the process of biological evolution, which is a global optimization

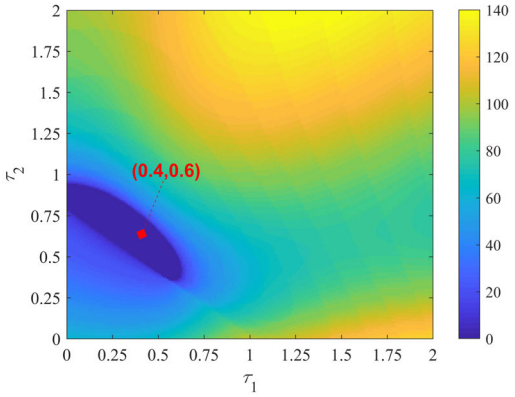

FIGURE 23. The stability chart of the controlled OVM with regard to τ_1 and τ_2 for $\gamma_1 = 0.7\ \mathrm{s}^{-1}$, $\gamma_2 = 0.9\ \mathrm{s}^{-1}$ and $\alpha = 0.7557\ \mathrm{s}^{-1}$.

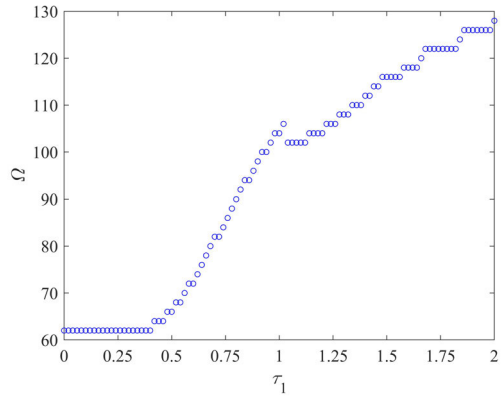

FIGURE 24. The stability chart of the controlled OVM with regard to τ_1 for $\gamma_1 = 0.7\ \mathrm{s}^{-1}$ and $\alpha = 0.7557\ \mathrm{s}^{-1}$.

search algorithm. The calibration process can be regarded as the process of solving the optimal solution of a nonlinear programming problem. Thereby, this paper leverages genetic algorithm to solve the optimal problem to achieve the goal of parameter calibration.

The objective function proposed by Ossen *et al.* [34] is taken and its expression is as follows:

$$\mathrm{PI} = \frac{\sqrt{\sum_{m=1}^{M}\left(a_m^{real} - a_m^{sim}\right)^2}}{\sqrt{\sum_{m=1}^{M}\left(a_m^{real}\right)^2} + \sqrt{\sum_{m=1}^{M}\left(a_m^{sim}\right)^2}} \tag{24}$$

where M denotes the sample size; m denotes the index number; a_m^{real} is the actual acceleration; a_m^{sim} is the simulated acceleration. The objective function (24) is taken as fitness function in GA. The smaller the value of fitness PI is, the better the parameter fitting effect.

The model to be calibrated are as follows:

$$\frac{dv_n(t)}{dt} = \alpha\left(V\left(\Delta x_n(t)\right) - v_n(t)\right) \tag{25}$$

$$V\left(\Delta x_n(t)\right) = V_0\left[\tanh(C_1(\Delta x_n(t) - h_c)) + C_2\right] \tag{26}$$

where the optimal velocity function is from Ref. [35], which has been toned for the convenience of calibration.

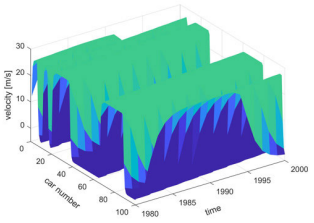

(a) Uncontrolled OVM

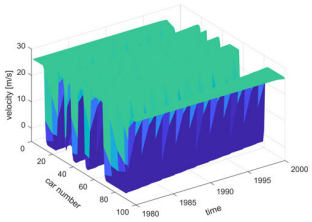

(b) Controlled OVM with single time-delay control

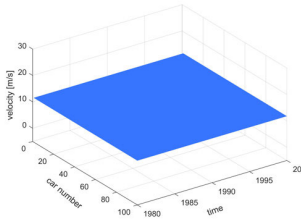

(c) Controlled OVM with double time-delay control

FIGURE 25. Comparison among the uncontrolled OVM (i.e. $\tau_1 = 0$ and $\tau_2 = 0$), the controlled OVM with single time-delay control (i.e. $\tau_1 = 0.4$ s and $\tau_2 = 0$ s) and the controlled OVM with double time-delay control (i.e. $\tau_1 = 0.4$ s and $\tau_2 = 0.6$ s) with fixed $\gamma_1 = 0.7\ \mathrm{s}^{-1}$, $\gamma_2 = 0.9\ \mathrm{s}^{-1}$ and $\alpha = 0.7557\ \mathrm{s}^{-1}$.

TABLE 1. The configuration of Genetic algorithm.

Option	Value
Population Size	100
Crossover Fraction	0.95
Migration Fraction	0.1
Generations	1000
TolFun	$1e-50$

TABLE 2. The range of calibrated parameters.

Symbol	Range
α	$[0,3]\ \mathrm{s}^{-1}$
h_c	$[5,35]$ m
V_0	$[15,40]$ m/s
C_1	$[0.05,2]$
C_2	$[0,1]$

The configuration of genetic algorithm is shown in Table 1 and the range of calibrated parameters is shown in Table 2.

Hence, the results of parameter calibration yield by performing GA, as shown in Table 3. In Fig. 22, the comparison between simulated accelerations and actual ones of dataset A illustrates that the fitting effect is acceptable.

After parameter calibration, we utilize dataset B to verify the results of calibration and obtain the evaluation value PI = 0.8042, which is within the acceptable range.

TABLE 3. The results of parameter calibration.

Symbol	Value
α	$0.7557\ \mathrm{s}^{-1}$
h_c	19.7760 m
V_0	15.0428 m/s
C_1	0.0874
C_2	0.7827
PI	0.5882

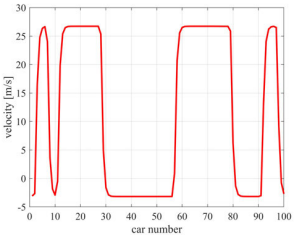

(a) Uncontrolled OVM

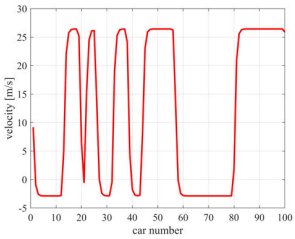

(b) Controlled OVM with single time-delay control

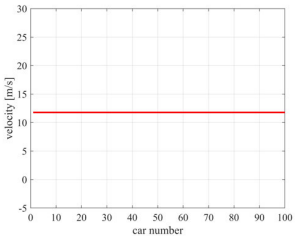

(c) Controlled OVM with double time-delay control

FIGURE 26. The snapshots of velocity for all vehicles at $t = 2000$ s correspond to Fig. 25.

3) DOUBLE TIME-DELAY CONTROL STRATEGY VERIFICATION

According to the abovementioned calibration, the OVM with double time-delay control reflecting actual traffic flow can be expressed as follows:

$$\frac{dv_n(t)}{dt} = 0.7557\,(V(\Delta x_n(t)) - v_n(t)) + \tilde{u}_n(t-\tau_1) + \tilde{e}_n(t-\tau_2) \quad (27)$$

$$\tilde{u}_n(t-\tau_1) = \gamma_1\,[v_n(t) - v_n(t-\tau_1)] \quad (28)$$

$$\tilde{e}_n(t-\tau_2) = \gamma_2\,[V(\Delta x_n(t)) - V(\Delta x_n(t-\tau_2))] \quad (29)$$

$$V(\Delta x_n(t)) = 15.0428\,[\tanh(0.0874(\Delta x_n(t) - 19.776)) + 0.7827] \quad (30)$$

where γ_1, γ_2, τ_1 and τ_2 are the parameters of the control signal we proposed, which are determined by the design of feedback control in Section IV. Subsequently, the same method as case 1 is applied to verify the design of delay control strategy based on measured data. Similarly, we select $N = 100$ vehicles on a 1977.6 m long circular road.

For fixed $\gamma_1 = 0.7\ \mathrm{s}^{-1}$, $\gamma_2 = 0.9\ \mathrm{s}^{-1}$ and $\alpha = 0.7557\ \mathrm{s}^{-1}$ corresponding to the unstable OVM (i.e. $\alpha < 2V' = 2.62948$), the stable region of the controlled OVM is determined in $(\tau_1, \tau_2) \in [0, 2] \times [0, 2]$, as shown in Fig. 23. Then,

we choose the parameter combination $(\tau_1, \tau_2) = (0.4, 0.6)$ in the stable region to validate the effect of the design of double time-delay control.

In order to more intuitively observe the superiority of double time-delay control compared to uncontrolled OVM and controlled OVM with single time-delay control, Fig. 25 and Fig. 26 are depicted. Obviously, compared with Fig. 25(a) and Fig. 25(b), the speed fluctuation of Fig. 25(c) is obviously suppressed, showing a stable state, which indicates that double time-delay control is more reliable than single time-delay control [19] under the same condition. Furthermore, from Fig. 24, it can be seen that there is no appropriate single time-delay control strategy to stabilize the traffic flow for $\gamma_1 = 0.7\ \mathrm{s}^{-1}$, which also demonstrates that the single time-delay control is short-sighted, that is, the narrower selection range is compared with the double time-delay control.

Through the above case analysis, the feasibility of practical application of double time-delay control strategy is verified, which also provides a novel idea for the design of vehicle assisted driving controllers.

VI. CONCLUSION

In this paper, a controlled OVM accounting for double time-delay control is proposed to dampen the unstable traffic oscillations generated by the uncontrolled OVM. Through stability analysis, the critical condition of bifurcation is given. Then, the definite integral method is presented, which is the core of design of double time-delay control. The application of the presented method to the study on the stability of the controlled OVM and the selection of the control parameters are performed, which further verifies the feasibility of the method and the rationality of the design. In the case study, more vehicles were considered and the measured data were also included, and the result of numerical simulation that the controlled OVM with reasonable parameter settings can smooth the traffic fluctuations caused by the uncontrolled OVM.

In addition to the research content mentioned above, this topic can also do the following further expansions:

(1) In this paper, the delay control strategy based on the definite integral method is only applied to suppress the unstable traffic oscillation caused by OVM, while how to apply it to other traffic models such as the intelligent driver model (IDM) [36] and Cooperative Adaptive Cruise Control (CACC) [37] is still a blank, which is a direction worth studying.

(2) The actual traffic data, such as NGSIM database, can be integrated into the future research. Some parameters in the traffic flow model can be calibrated by leveraging the measured data, by which stability control parameters determined will have more practical application value.

(3) Due to the universal applicability of the definite integral method, the double time-delay feedback control can be extended to the n-dimensional time-delay feedback control, which is difficult to achieve for the previous single time-delay control.

APPENDIX
THE SPECIFIC PROCEDURE OF THE IMPROVED DEFINITE INTEGRAL METHOD

Step 1. Inserting $\lambda = i\omega$ into (21) and separating the real part of $i^{-n}f(i\omega)$ yields:

$$R(\omega) = \mathrm{Re}\left(i^{-n}f(i\omega)\right) = \omega^2 - \gamma_1\omega s_{\tau 1} - \beta + \delta c_{\tau 2} + \beta c_k - \delta c_{\tau 2}c_k - \delta s_{\tau 2}s_k \quad \text{(A1)}$$

where n represents the highest degree of the characteristic equation (21).

Step 2. According to (A1), all positive roots $W = \{\omega_1, \omega_2, \ldots, \omega_m\}$ of $R(\omega) = 0$ are solved. Take the maximum value of the set W as $\omega_{\max}$, and select arbitrary $T_0 > \omega_{\max}$ as the upper limit of definite integral.

Step 3. In the light of $\Re(\omega) = \mathrm{Re}\left(f'(i\omega)/f(i\omega)\right)$, the integrand $\Re(\omega)$ yields:

$$\Re(\omega) = \mathrm{Re}\left(\frac{f'(i\omega)}{f(i\omega)}\right) = \frac{\mathrm{Re}\left(f'(i\omega)\right)\mathrm{Re}(f(i\omega)) + \mathrm{Im}\left(f'(i\omega)\right)\mathrm{Im}(f(i\omega))}{[\mathrm{Re}(f(i\omega))]^2 + [\mathrm{Im}(f(i\omega))]^2} \quad \text{(A2)}$$

where $\mathrm{Re}\left(f'(i\omega)\right)$ is the real part of $f'(i\omega)$ whose expression as follows:

$$\mathrm{Re}\left(f'(i\omega)\right) = -\varepsilon + \gamma_1 c_{\tau 1} - \gamma_1\tau_1 s_{\tau 1} + \tau_2\delta c_{\tau 2} - \tau_2\delta c_{\tau 2}c_k - \tau_2\delta s_{\tau 2}s_k; \quad \text{(A3)}$$

$\mathrm{Im}\left(f'(i\omega)\right)$ is the imaginary part of $f'(i\omega)$ and its expression as below:

$$\mathrm{Im}\left(f'(i\omega)\right) = 2\omega - \gamma_1 s_{\tau 1} - \gamma_1\tau_1\omega c_{\tau 1} - \tau_2\delta s_{\tau 2} - \tau_2\delta c_{\tau 2}s_k + \tau_2\delta s_{\tau 2}c_k; \quad \text{(A4)}$$

The real part of $f(i\omega)$ is recorded as $\mathrm{Re}(f(i\omega))$:

$$\mathrm{Re}(f(i\omega)) = -\omega^2 + \gamma_1\omega s_{\tau 1} + \beta - \delta c_{\tau 2} - \beta c_k + \delta c_{\tau 2}c_k + \delta s_{\tau 2}s_k; \quad \text{(A5)}$$

The imaginary part of $f(i\omega)$ is marked as $\mathrm{Im}(f(i\omega))$:

$$\mathrm{Im}(f(i\omega)) = -\varepsilon\omega + \gamma_1\omega c_\tau^1 + \delta s_\tau^2 - \beta s_k + \delta c_\tau^2 s_k - \delta s_\tau^2 c_k. \quad \text{(A6)}$$

Step 4. Introducing T_0 in Step 2 and integrand $\Re(\omega)$ in Step 3 into the following definite integral yields:

$$F(0, T_0)_k = \int_0^{T_0} \Re(\omega)d\omega \quad \text{(A7)}$$

For every k and $k \neq N$, total number $\Omega_k(\tau_1, \tau_2)$ of eigenvalues with positive real part yields by:

$$\Omega_k(\tau_1, \tau_2) = \mathrm{round}\left(\frac{n}{2} - \frac{F(0, T_0)_k}{\pi}\right) \quad \text{(A8)}$$

Step 5. Sum the $\Omega_k(\tau_1, \tau_2)$ for every k and $k \neq N$, that is, $\Omega(\tau_1, \tau_2) = \sum_{k=1}^{N-1}\Omega_k(\tau_1, \tau_2)$. If $\Omega(\tau_1, \tau_2) = 0$, the system (4) with τ_1 and τ_2 is stable. Otherwise, $\Omega(\tau_1, \tau_2) \neq 0$ means there exists bifurcation in the system (4).

REFERENCES

[1] S. Li, L. Yang, Z. Gao, and K. Li, "Stabilization strategies of a general nonlinear car-following model with varying reaction-time delay of the drivers," *ISA Trans.*, vol. 53, no. 6, pp. 1739–1745, Nov. 2014.
[2] D. Sun, D. Chen, M. Zhao, W. Liu, and L. Zheng, "Linear stability and nonlinear analyses of traffic waves for the general nonlinear car-following model with multi-time delays," *Phys. A, Stat. Mech. Appl.*, vol. 501, pp. 293–307, Jul. 2018.
[3] G. Zhang, Y. Zhang, D.-B. Pan, and C.-Y. Sang, "Study on the interval integration effect of vehicle's self-delayed velocity on traffic stability in micro traffic modeling," *Phys. A, Stat. Mech. Appl.*, vol. 533, Nov. 2019, Art. no. 121941.
[4] D. Ngoduy, "Generalized macroscopic traffic model with time delay," *Nonlinear Dyn.*, vol. 77, nos. 1–2, pp. 289–296, Jul. 2014.
[5] R. G. Xu, "Multiple traffic jams in full velocity difference model with reaction-time delay," *Int. J. Simul. Model.*, vol. 14, no. 2, pp. 325–334, Jun. 2015.
[6] Y. Mei, X. Zhao, Y. Qian, S. Xu, Y. Ni, and Z. Li, "Analyses of self-stabilizing control strategy effect in macroscopic traffic model by utilizing historical velocity data," *Commun. Nonlinear Sci. Numer. Simul.*, vol. 74, pp. 55–68, Jul. 2019.
[7] Z. Min, S. Di-Hua, and T. Chuan, "An extended two-lane traffic flow lattice model with driver's delay time," *Nonlinear Dyn.*, vol. 77, no. 3, pp. 839–847, Aug. 2014.
[8] G. Zhang, "Study on varying time delay on traffic stability in a novel lattice hydrodynamic model," *Phys. A, Stat. Mech. Appl.*, vol. 505, pp. 1103–1112, Sep. 2018.
[9] R. E. Chandler, R. Herman, and E. W. Montroll, "Traffic dynamics: Studies in car following," *Oper. Res.*, vol. 6, no. 2, pp. 165–184, Apr. 1958.
[10] L. A. Pipes, "An operational analysis of traffic dynamics," *J. Appl. Phys.*, vol. 24, no. 3, pp. 274–281, Mar. 1953.
[11] M. Bando, K. Hasebe, A. Nakayama, A. Shibata, and Y. Sugiyama, "Dynamical model of traffic congestion and numerical simulation," *Phys. Rev. E, Stat. Phys. Plasmas Fluids Relat. Interdiscip. Top.*, vol. 51, no. 2, pp. 1035–1042, Feb. 1995.
[12] Y. Igarashi, K. Itoh, K. Nakanishi, K. Ogura, and K. Yokokawa, "Bifurcation phenomena in the optimal velocity model for traffic flow," *Phys. Rev. E, Stat. Phys. Plasmas Fluids Relat. Interdiscip. Top.*, vol. 64, no. 4, Sep. 2001, Art. no. 047102.
[13] G. Orosz, B. Krauskopf, and R. E. Wilson, "Bifurcations and multiple traffic jams in a car-following model with reaction-time delay," *Phys. D, Nonlinear Phenomena*, vol. 211, nos. 3–4, pp. 277–293, Nov. 2005.
[14] I. Gasser, T. Seidel, G. Sirito, and B. Werner, "Bifurcation analysis of a class of car following traffic models II: Variable reaction times aggressive drivers," *Bull. Inst. Math. Academia Sinica*, vol. 2, no. 2, pp. 587–607, Jun. 2007.
[15] G. K. Kamath, K. Jagannathan, and G. Raina, "Car-following models with delayed feedback: Local stability and hopf bifurcation," in *Proc. 53rd Annu. Allerton Conf. Commun., Control, Comput. (Allerton)*, Springfield, IL, USA, Sep. 2015, pp. 538–545.
[16] Y. Zhang, Y. Xue, P. Zhang, D. Fan, and H. di He, "Bifurcation analysis of traffic flow through an improved car-following model considering the time-delayed velocity difference," *Phys. A, Stat. Mech. Appl.*, vol. 514, pp. 133–140, Jan. 2019.
[17] Y. Jin and H. Hu, "Stabilization of traffic flow in optimal velocity model via delayed-feedback control," *Commun. Nonlinear Sci. Numer. Simul.*, vol. 18, no. 4, pp. 1027–1034, Apr. 2013.
[18] G. Peng, S. Yang, D. Xia, and X. Li, "Delayed-feedback control in a car-following model with the combination of V2V communication," *Phys. A, Stat. Mech. Appl.*, vol. 526, Jul. 2019, Art. no. 120912.
[19] Y. Jin and J. Meng, "Dynamical analysis of an optimal velocity model with time-delayed feedback control," *Commun. Nonlinear Sci. Numer. Simul.*, vol. 90, Nov. 2020, Art. no. 105333.
[20] K. Konishi, H. Kokame, and K. Hirata, "Coupled map car following model and its delayed-feedback control," *Phys. Rev. E, Stat. Phys. Plasmas Fluids Relat. Interdiscip. Top.*, vol. 60, no. 4, pp. 4000–4007, Oct. 1999.
[21] Z. Li, Q. Qin, W. Li, S. Xu, Y. Qian, and J. Sun, "Stabilization analysis and modified KdV equation of a car-following model with consideration of self-stabilizing control in historical traffic data," *Nonlinear Dyn.*, vol. 91, no. 2, pp. 1113–1125, Jan. 2018.
[22] I. Hashlamon, "A new adaptive extended Kalman filter for a class of nonlinear systems," *J. Appl. Comput. Mech.*, vol. 6, no. 1, pp. 1–12, 2019.
[23] S. He, W. Lyu, and F. Liu, "Robust H_∞ sliding mode controller design of a class of time-delayed discrete conic-type nonlinear systems," *IEEE Trans. Syst., Man, Cybern., Syst.*, early access, doi: 10.1109/TSMC.2018.2884491.
[24] R. Nie, S. He, F. Liu, and X. Luan, "Sliding mode controller design for conic-type nonlinear semi-Markovian jumping systems of time-delayed Chua's circuit," *IEEE Trans. Syst., Man, Cybern., Syst.*, early access, doi: 10.1109/TSMC.2019.2914491.
[25] S. He, Q. Ai, C. Ren, J. Dong, and F. Liu, "Finite-time resilient controller design of a class of uncertain nonlinear systems with time-delays under asynchronous switching," *IEEE Trans. Syst., Man, Cybern., Syst.*, vol. 49, no. 2, pp. 281–286, Feb. 2019.
[26] Q. Xu, G. Stepan, and Z. Wang, "Delay-dependent stability analysis by using delay-independent integral evaluation," *Automatica*, vol. 70, pp. 153–157, Aug. 2016.
[27] M. Fu, A. W. Olbrot, and M. Polis, "Robust stability for time-delay systems: The edge theorem and graphical test," *IEEE Trans. Autom. Control*, vol. 34, pp. 813–820, Dec. 1989.
[28] V. Kolmanovskii, and A. Myshkis, *Introduction to the Theory and Applications of Function Differential Equations*. Dordrecht, The Netherlands: Kluwer, 1999.
[29] C. Chen, L. Li, J. Hu, and C. Geng, "Calibration of MITSIM and IDM car-following model based on NGSIM trajectory datasets," in *Proc. IEEE Int. Conf. Veh. Electron. Saf.*, Jul. 2010, pp. 48–53.
[30] D. H. Wang, P. F. Tao, S. Jin, and D. F. Ma, "Method of calibrating and validating car-following model," *J. Jilin Univ.*, vol. 41, no. S1, pp. 59–65, Jul. 2011.
[31] S. P. Hoogendoorn and R. Hoogendoorn, "Generic calibration framework for joint estimation of car-following models by using microscopic data," *Transp. Res. Rec., J. Transp. Res. Board*, vol. 2188, no. 1, pp. 37–45, Jan. 2010.
[32] T. Ma and B. Abdulhai, "Genetic algorithm-based optimization approach and generic tool for calibrating traffic microscopic simulation parameters," *Transp. Res. Rec., J. Transp. Res. Board*, vol. 1800, no. 1, pp. 6–15, Jan. 2002.
[33] L. Zheng, Z. He, and T. He, "An anisotropic continuum model and its calibration with an improved monkey algorithm," *Transportmetrica A, Transp. Sci.*, vol. 13, no. 6, pp. 519–543, Jul. 2017.
[34] S. J. Ossen, S. P. Hoogendoorn, and B. G. Gorte, "Interdriver differences in car-following: A vehicle trajectory–based study," *Transp. Res. Rec.*, vol. 1965, no. 1, pp. 121–129, 2007.
[35] L. C. Davis, "Modifications of the optimal velocity traffic model to include delay due to driver reaction time," *Phys. A, Stat. Mech. Appl.*, vol. 319, pp. 557–567, Mar. 2003.
[36] M. Treiber, A. Hennecke, and D. Helbing, "Congested traffic states in empirical observations and microscopic simulations," *Phys. Rev. E, Stat. Phys. Plasmas Fluids Relat. Interdiscip. Top.*, vol. 62, no. 2, pp. 1805–1824, Aug. 2000.
[37] V. Milanés and S. E. Shladover, "Modeling cooperative and autonomous adaptive cruise control dynamic responses using experimental data," *Transp. Res. C, Emerg. Technol.*, vol. 48, pp. 285–300, Nov. 2014.

WEILIN REN was born in Nantong, Jiangsu, China, in 1997. He received the B.E. degree in traffic engineering from Jiangsu University, Zhenjiang, China, in 2019. He is currently pursuing the master's degree in port and waterway technology and management engineering with Ningbo University. His research interests include traffic flow modeling and bifurcation analysis.

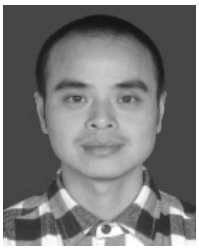

RONGJUN CHENG received the B.S. and M.S. degrees in math from Anhui Normal University, in 1999 and 2004, respectively, and the Ph.D. degree in mechanic from Shanghai University, in 2007. He is currently a Professor with Ningbo University. He has published more than 100 articles indexed by SCI. His research interests include traffic flow modeling, transportation safety, intelligent transportation systems, and meshless method.

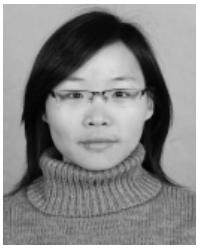

HONGXIA GE received the B.S. degree in traffic engineering from Anhui Normal University, in 2000, and the Ph.D. degree in transportation from Shanghai University, in 2006. She is currently a Professor with Ningbo University. She has published more than 100 articles indexed by SCI. Her research interests include traffic flow modeling and density wave analysis.

QI WEI was born in Ningbo, Zhejiang, China, in 1980. He received the M.S. degree in operational research and cybernetics from Zhejiang University, China, in 2006, and the Ph.D. degree in operational research and cybernetics from Shanghai University, Shanghai, China, in 2015. From 2006 to 2016, he was a Lecturer with the Ningbo Institute of Technology, Zhejiang University. Since 2016, he has been an Associate Professor with the Ningbo University of Finance and Economics. He is the author of more than 20 articles. His research interests include computational complexity, algorithm design, game theory, and scheduling.